Inorganic Chemistry

Article

pubs.acs.org/IC

Hydrothermal Synthesis of Yttria-Stabilized Zirconia Nanocrystals with Controlled Yttria Content

Kazuyoshi Sato,*[,†] Kazuya Horiguchi,[†] Taku Nishikawa,[‡] Sadahiro Yagishita,[‡] Kazuo Kuruma,[§] Takeshi Murakami,[§] and Hiroya Abe[§]

[†]Division of Environmental Engineering Science, Graduate School of Science and Technology, Gunma University, 1-5-1 Tenjin-cho, Kiryu, Gunma 376-8515 Japan

[‡]Daiichi Kigenso Kagaku Kogyo Co., Ltd, 1-6-38, Hirabayashi-minami, Suminoe, Osaka 559-0025 Japan

[§]Joining and Welding Research Institute, Osaka University, 11-1 Mihogaoka, Ibaraki, Osaka 567-0047 Japan

Supporting Information

ABSTRACT: In this study, we demonstrate for the first time the hydrothermal synthesis of yttria-stabilized zirconia (YSZ) nanocrystals with controlled yttria content (x = 3−12 mol %; xYSZ) with negligible aggregation from aqueous solution. The nanocrystals were grown via the hydrothermal treatment of basic Zr(IV) and Y(III) carbonate complex aqueous solutions in the presence of a cationic ligand, $N(CH_3)_4^+$. The nanocrystals were characterized in detail by dynamic light scattering, ζ-potential measurement, X-ray diffraction, specific surface area measurement based on the Brunauer−Emmett−Teller theory, transmission electron microscopy, energy dispersive X-ray spectroscopy, and Raman spectroscopy. Shorter reaction times and higher Y_2O_3 content produce aqueous solutions with higher transparencies containing nanocrystals with sizes of 10 nm or less. Nanocrystals with the target composition were obtained by hydrothermal reaction for longer than 3 h, regardless of the Y_2O_3 content. The main phase is tetragonal for (3−6)YSZ and cubic with disordered oxygen vacancies for (8−12)YSZ. The characteristics of the nanocrystalline material synthesized are consistent with those of bulk YSZ crystals, indicating the growth of high-quality nanocrystals.

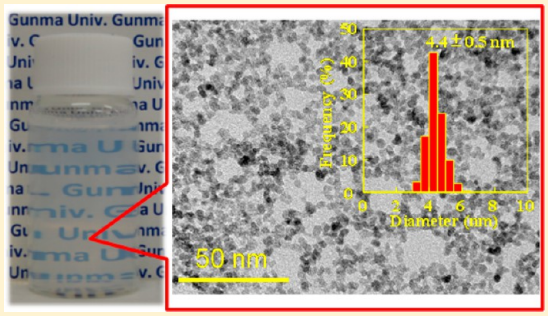

1. INTRODUCTION

The high-temperature forms (tetragonal and cubic) of zirconia (ZrO_2) are stabilized even at room-temperature by doping with yttria (Y_2O_3). Yttria-stabilized zirconia (YSZ) is an important ceramic material because of its great potential for use in several applications including oxygen sensors,[1] solid oxide fuel cell (SOFC) electrolytes,[2] and phase-transformation-toughened structural materials.[3] These applications depend on the physicochemical properties of YSZ, which are tunable by varying the Y_2O_3 doping level. In addition, the fabrication of uniform nanocomposites of YSZ with other metals and oxides enhances the performance and extends their range of applications. For instance, Al_2O_3/tetragonal YSZ composites exhibit significantly enhanced mechanical properties compared with monolithic Al_2O_3 and tetragonal YSZ ceramics,[4] and Sr-doped $LaMnO_3$/cubic YSZ and Ni/cubic YSZ composites are promising candidates for SOFC electrodes.[5,6]

The growth of nanocrystals in an aqueous medium offers great advantages for fabricating composites.[7,8] Low-temperature liquid-phase processes are attractive because they provide the controllable nucleation, crystallization, and growth in one-pot. Moreover, the aid of organic molecules is available because the growth of crystalline oxides can be achieved below the decomposition temperature of the molecules. Goto et al. have successfully grown YSZ nanocrystals of varying Y_2O_3 contents through a nonhydrolytic sol−gel approach.[9] However, the nanocrystals could not be dispersed in an aqueous medium due to surface capping with hydrophobic oleylamine. Although Liu et al. reported that water-dispersible lanthanide (Eu^{3+} and Tb^{3+})-doped ZrO_2 nanocrystals can be obtained using a solvothermal approach, continuous washing and ligand exchange sequences are required.[10] Recently, Guiot et al. successfully grew water-dispersible 9-mol %-Y_2O_3-doped ZrO_2 ($Zr_{0.83}Y_{0.17}O_{1.915}$) nanocrystals via hydrothermal treatment.[11] However, only 40% of the soluble Y^{3+} is converted into the solid phase, even with a long reaction time of 3 days at 160 °C.

Recently, the authors reported that aqueous dispersions of high-quality oxide nanocrystals can be obtained through a modified hydrothermal method.[12−14] The key to this approach is the preparation of metastable, water-soluble anionic complex in a basic solution as the precursor. In addition, $N(CH_3)_4^+$, which caps surface oxygen sites, controls the growth behavior and helps control nanocrystal aggregation during the hydrothermal treatment.[12] This approach should also be applicable to the growth of YSZ nanocrystals from aqueous dispersions

Received: May 19, 2015
Published: July 31, 2015

DOI: 10.1021/acs.inorgchem.5b01112
Inorg. Chem. 2015, 54, 7976−7984

because Zr(VI) and Y(III) both form aqueous anionic carbonate complexes in the presence of excess CO_3^{2-}.[15,16] The goal of this study was to (1) synthesize YSZ nanocrystals with varying yttria content from aqueous solutions and (2) characterize those nanocrystals in detail to better understand the fundamental aspects of the synthesis of aqueous dispersions of various trivalent lanthanide (Ln^{3+})-doped ZrO_2 nanocrystals using this synthesis approach, since a variety of Ln^{3+} form similar anionic carbonate complexes.

2. EXPERIMENTAL SECTION

2.1. Hydrothermal Growth of YSZ Nanocrystals of Varying Y_2O_3 Content. YSZ nanocrystals of varying Y_2O_3 content (3, 6, 8, 10, and 12 mol %) were hydrothermally grown according to the protocol shown in Figure 1. In the remaining text, the samples are denoted as

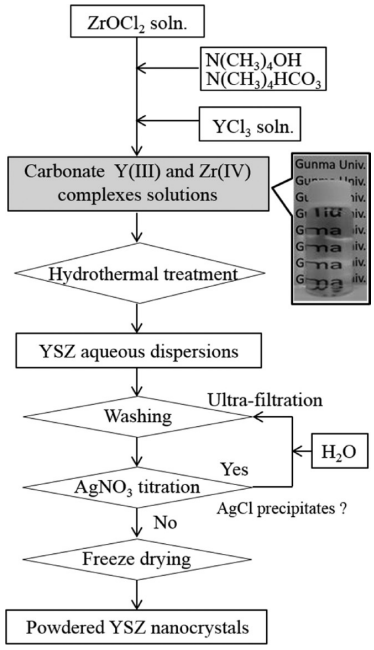

Figure 1. Process flow diagram for producing YSZ nanocrystals.

*x*YSZ, where *x* is the mol % of Y_2O_3. The aqueous basic Zr(IV) and Y(III) carbonate complexes solution (the amount of total cations of 0.1 mol) were prepared as the precursor of YSZ nanocrystals through the following sequence; the mixed aqueous solution of 25 wt % $N(CH_3)_4OH$ (tetramethylammonium hydroxide; TMAH) and 67 wt %$N(CH_3)_4HCO_3$ (tetramethylammonium hydrogen carbonate; TMAHC) was added into $ZrOCl_2$ aqueous solution, and then, YCl_3 aqueous solution was added to the Zr(IV) complexes solution. The optimal amount of both TMAH and TMAHC solutions determined by preliminary experiments was 15 mL each. The total amount of 50 mL of complex solution (metal ion concentration of 0.2 mol·L^{-1}) was enclosed in a polytetrafluoroethylene (PTFE)-lined stainless-steel autoclave and heat treated at 150 °C for 1−24 h in an oven and then cooled to room temperature. The Cl^-, excess $N(CH_3)_4^+$, and the soluble cations that were not converted to a solid were removed by ultrafiltration with a molecular weight cutoff of 5000. The washing sequence was continued until the major anion, Cl^-, was removed. The completion of the washing sequence was confirmed through $AgNO_3$ titration ($AgNO_3 + Cl^- \rightarrow AgCl + NO_3^-$) of the ultrafiltrated solution. The YSZ nanocrystals were then obtained. A portion of the nanocrystals was freeze-dried to obtain powdered YSZ nanocrystals for subsequent characterization.

2.2. Characterization of YSZ Nanocrystals. The crystalline phase of the powdered YSZ nanocrystals was characterized by powder X-ray diffraction (XRD) using Cu Kα radiation (λ = 0.1542 nm). The crystallite size was estimated from the full-width at half maximum (FWHM) of a diffraction peak using the Scherrer equation.[17] The Y_2O_3 doping level in the nanocrystals was evaluated by energy dispersive X-ray spectroscopy (EDS) using the calibration curve method. A rhodium target was employed for the excitation of fluorescent X-rays. The morphologies and size distribution of the YSZ nanocrystals were characterized using transmission electron microscopy (TEM) with an acceleration voltage of 200 kV. The size distributions of the nanocrystals in the aqueous solution (hydrodynamic diameters) were measured by dynamic light scatting (DLS). Specific surface area (SSA_{BET}) was measured on the basis of Brunauer−Emmet−Teller (BET) theory[18] from N_2 gas adsorption isotherms measured at 77 K. The local structures of the nanocrystals such as order−disorder effects of the oxygen sublattice were investigated by Raman spectroscopy. A continuous wave with a wavelength of 325 nm was employed as the excitation line.

3. RESULTS AND DISCUSSION

Figure 2 shows the appearances of the YSZ nanocrystal aqueous dispersions as a function of reaction time. Shorter

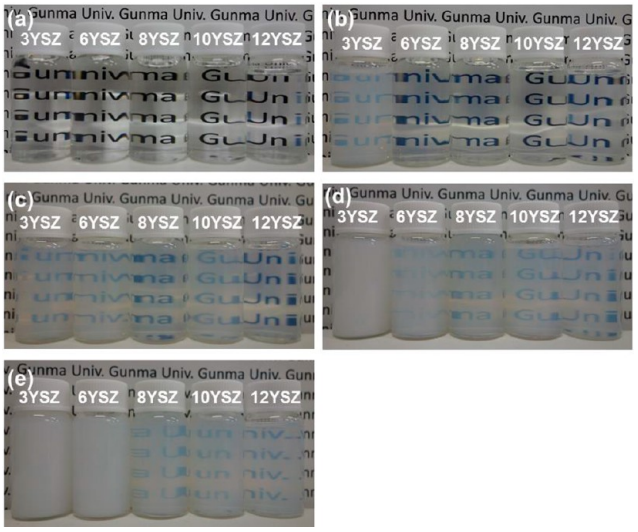

Figure 2. Appearance of aqueous dispersions of YSZ nanocrystals with varying Y_2O_3 content grown at 150 °C for (a) 1 h, (b) 3 h, (c) 6 h, (d) 12 h, and (e) 24 h.

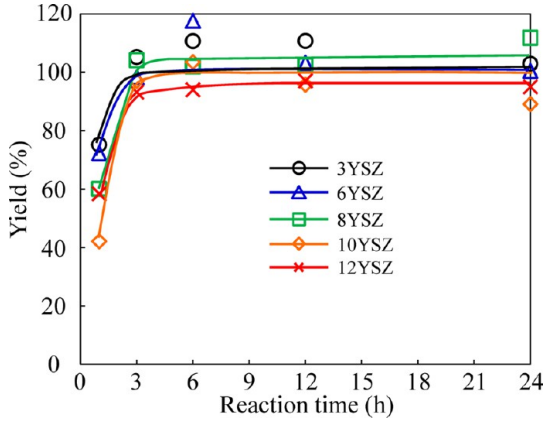

Figure 3. Effect of hydrothermal reaction time on yield of YSZ nanocrystals.

reaction times and higher Y_2O_3 content provided solutions with better transparencies. The nanocrystal yield evaluated from the mass of the solid product was <80% after hydrothermal

DOI: 10.1021/acs.inorgchem.5b01112
Inorg. Chem. 2015, 54, 7976−7984

Table 1. Summary of Hydrodynamic Diameters of YSZ Nanocrystals Grown at 150 °C for (a) 3 h, (b) 6 h, (c) 12 h, and (d) 24 h

	(a)				
	3YSZ	6YSZ	8YSZ	10YSZ	12YSZ
D_{10} (nm)	19.5	10.3	9.13	8.73	10.8
D_{50} (nm)	28.2	16.1	13.5	13.2	16.2
D_{90} (nm)	50.8	28.1	23.3	22.9	27.9
	(b)				
	3YSZ	6YSZ	8YSZ	10YSZ	12YSZ
D_{10} (nm)	37.4	17.6	17.7	24.7	14.7
D_{50} (nm)	59.6	29.2	27.2	37.8	23.4
D_{90} (nm)	125	57.0	47.6	66.6	42.3
	(c)				
	3YSZ	6YSZ	8YSZ	10YSZ	12YSZ
D_{10} (nm)	35.8	33.9	30.7	32.7	24.0
D_{50} (nm)	55.12	52.8	46.4	49.6	37.4
D_{90} (nm)	106	96.1	81.2	89.0	70.5
	(d)				
	3YSZ	6YSZ	8YSZ	10YSZ	12YSZ
D_{10} (nm)	58.1	47.8	35.9	36.1	38.4
D_{50} (nm)	95.4	78.6	54.6	55.4	59.2
D_{90} (nm)	207	168	95.3	99.1	114

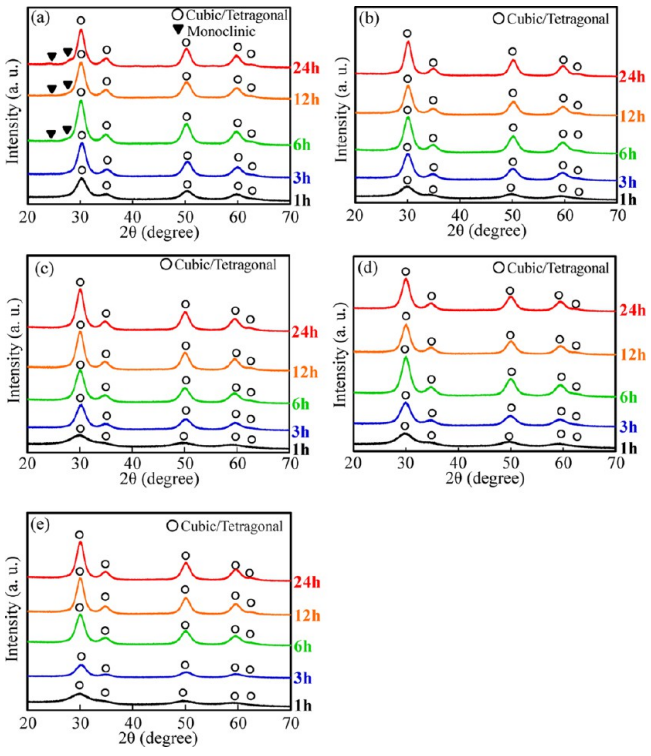

Figure 4. XRD patterns of YSZ nanocrystals with varying Y_2O_3 content grown at 150 °C for (a) 1 h, (b) 3 h, (c) 6 h, (d) 12 h, and (e) 24 h.

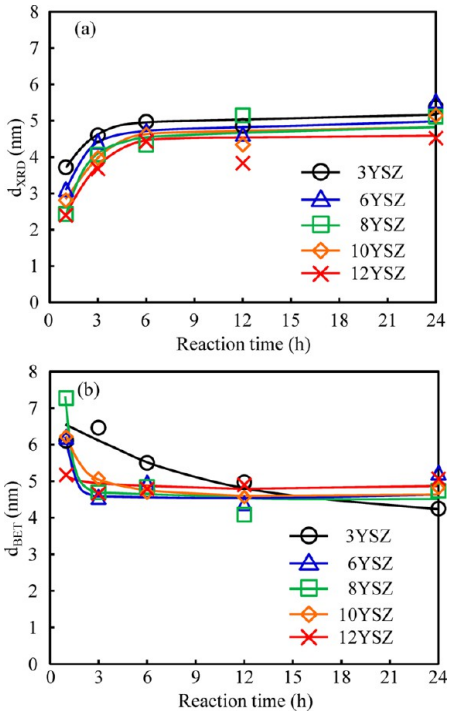

Figure 5. (a) Crystalline sizes estimated from the XRD (d_{XRD}) and (b) equivalent particle diameters calculated from the SSA_{BET} (d_{BET}) data of the YSZ nanocrystals with varying Y_2O_3 content grown at 150 °C for 1−24 h.

treatment for 1 h and approaches nearly 100% after 3 h independent of the composition (Figure 3). The transparency of the solution is attributed to the nanosize of the particles and that there is likely minimal particle agglomeration such that Mie scattering of visible light is minimal.[19] The decreased transparencies of the sample by increasing reaction time above 3 h even though the solid content is constant (see Figure 3) may be attributed to significant Mie scattering by large particles with the size similar to the wavelength of visible light. The fact strongly suggests that significant growth or agglomeration of the primary nanocrystals occurs by increasing reaction time. However, the size is small enough to prevent sedimentation since no solid−liquid phase separation was observed, even in those samples. Figure 3 also indicates that both Y^{3+} and Zr^{4+} species were almost completely converted into the solid phase during hydrothermal treatment at 150 °C for longer than 3 h. The yield is quite high compared with the hydrothermal approach reported by Guiot et al., where only 40% of yttrium was converted into the solid, even after hydrothermal treatment at 160 °C for 3 days.[11] They chose pH 7 as reaction environment and yttrium hydroxide as precursor. However, yttrium hydroxide is thermodynamically unstable at pH 7 and most of it will be decomposed into Y^{3+} and OH^- rather than converted into solid oxide.[20] The higher yield in this study may be attributed to the basic environment of the hydrothermal treatment, which prevented the dissolution of Y^{3+}-containing solids such as hydroxides, carbonates, and oxides.

Table 1 shows the YSZ nanocrystal size distribution in the colloidal solutions as a function of Y_2O_3 content and reaction time. All the samples have unimodal and narrow size distributions, which can be attributed to the separated nucleation and growth processes of the nanocrystals.[21] Significant crystal growth occurs in the conventional approach due to occurrence of simultaneous nucleation and growth, where material sources are divided between the small number of nuclei. In contrast, materials are mainly consumed for nuclei formation rather than crystal growth since capping agent restricts incorporation of sources into nuclei, thereby the amount of materials divided between each nuclei decreases,

DOI: 10.1021/acs.inorgchem.5b01112
Inorg. Chem. 2015, 54, 7976−7984

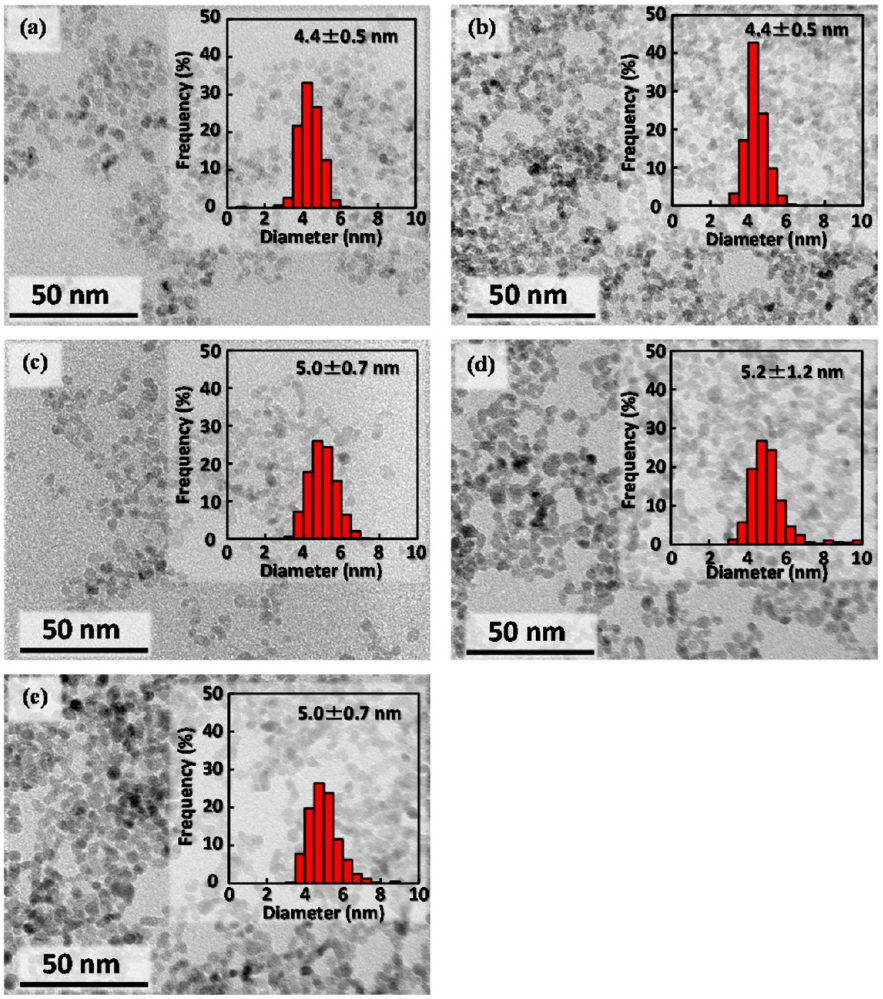

Figure 6. TEM images and corresponding particle size distributions of 8YSZ nanocrystals grown at 150 °C for (a) 1 h, (b) 3 h, (c) 6 h, (d) 12 h, and (e) 24 h.

resulting in minimal crystal growth in the present approach. Furthermore, the size of the nanocrystals is kept small due to the prevented dissolution of the nanocrystals by capping, which is the driving force of Ostwald ripening.[13]

The average size of nanocrystals synthesized after 3 h is in the range of 13−18 nm with the exception of 3YSZ, suggesting that the nanocrystals are approximately 10 nm or less in size since hydrodynamic diameter overestimates the real size of particles by several nanometers and it involves the size of the inorganic core, surface capping agent, and solvation (hydration) layer.[14] The size of $N(CH_3)_4^+$ is approximately 0.7 nm in diameter, and solvation layer is commonly a few nm.[22]

Figure 4 shows the evolution of the crystalline phase of the YSZ nanocrystals of varying Y_2O_3 content as a function of reaction time. The crystalline phase mainly consists of fluorite-type ZrO_2 with tetragonal or cubic crystallographic symmetry. Although it is impossible to distinguish between the tetragonal and cubic phases from the data since significant peak broadening masks the characteristic peak splitting of the tetragonal phase, the stabilization of the tetragonal or cubic phase strongly suggests that Y_2O_3 was successfully doped into the nanocrystal lattices since the pure monoclinic phase was obtained when pure ZrO_2 nanocrystals were grown using this approach.[12]

Shortening the reaction time and increasing the Y_2O_3 content broadens the diffraction peaks, which can be attributed to smaller crystalline size and/or lattice strain. Some minor peaks assigned to the monoclinic phase are observed in 3YSZ grown for longer than 6 h; these peaks become more intense with increasing reaction time. This phenomenon may be attributed to spontaneous transformation of metastable tetragonal phase to monoclinic phase under hydrothermal environment, referred to as hydrothermal degradation.[23]

Figure 5 compares the crystalline size (d_{XRD}) estimated on the basis of the peak broadening of XRD patterns (Figure 4) and the equivalent particle diameter (d_{BET}) calculated from the SSA_{BET} data (Figure S-2, Supporting Information) as functions of reaction time. The d_{BET} was calculated using the following equation:

$$d_{BET} = 6/(\rho_{th} SSA_{BET})$$

where ρ_{th} is the theoretical density of YSZ.[24]

The d_{XRD} increases with increasing reaction time up to 6 h and then remains almost constant up to 24 h independent of Y_2O_3 content; d_{XRD} ranged from 2 to 4 nm at 1 h, increased to approximately 4−5 nm at 6 h, and then remained constant. In contrast, d_{BET} decreases with increasing reaction time up to 3 h and then remains almost constant up to 24 h; d_{BET} was in the range of 5−7.5 nm at 1 h and decreased to approximately 4−5

DOI: 10.1021/acs.inorgchem.5b01112
Inorg. Chem. 2015, 54, 7976−7984

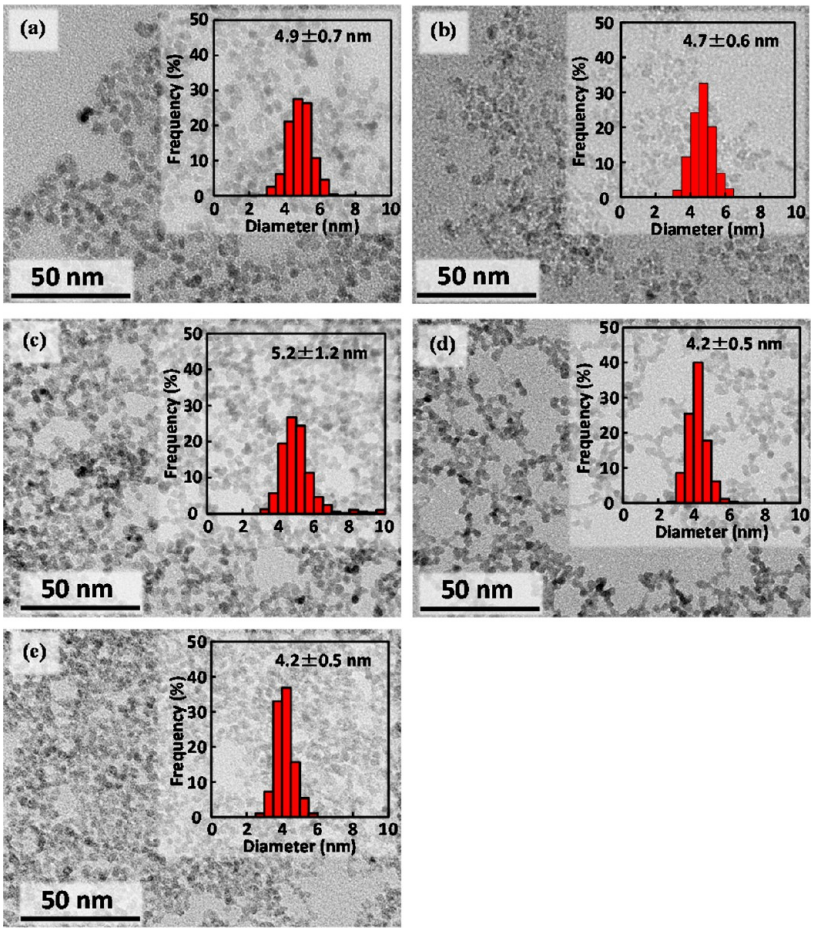

Figure 7. TEM images and corresponding particle size distributions of (a) 3YSZ, (b) 6YSZ, (c) 8YSZ, (d) 10YSZ, and (e) 12 YSZ nanocrystals grown at 150 °C for 3 h.

nm above 6 h. The larger d_{BET} at 1 h may be attributed to the formation of solid bridges between nanocrystals through condensation of soluble Y(III) and Zr(IV) species unremovable by the washing sequences and subsequent precipitation of them as solid product during drying since measurable amounts of unreacted species are present in the aqueous solutions (Figure 3). The almost constant values of d_{XRD} and d_{BET} above 6 h along with their good agreement strongly suggests that nanocrystals with diameters of 4−5 nm were formed and only loosely agglomerated, which permitted adsorbent (N_2) permeation into small interstices between the nanocrystals, even in opaque samples shown in Figure 2.

Figure 6 shows the morphological changes in 8YSZ nanocrystals with reaction time. The nanocrystals are equiaxial in shape, and no abnormally large crystal was observed. The size distribution evaluated by TEM reveals that the primary nanocrystal size only slightly increases with increasing reaction time below 6 h and then remains constant up to 24 h. Furthermore, the average size of 4.4 ± 0.5 nm is remarkably larger than the d_{XRD} of the sample grown for 1 h (2.4 nm), while the size of approximately 5 nm was in good agreement with the d_{XRD} and d_{BET} values of crystals grown for more than 6 h. These results indicate that the significant XRD peak broadening for the nanocrystals grown for 1 h compared with those grown for longer periods of time is mainly attributed to lattice strain rather than smaller crystallite size. In contrast, the good agreement of the average size with d_{XRD} values for samples grown for more than 6 h strongly suggests the relaxation of the lattice strain. The formation of a significant amount of lattice strain at the early stage of reaction and its relaxation with increasing reaction time is shown and discussed later.

The significantly larger particle size in DLS measurement (see Table 1) compared to d_{BET} and d_{XRD} as well as the primary nanocrystal size determined by TEM indicates that the nanocrystals agglomerate and cause significant light scattering for the sample with cloudy appearances in Figure 2.

Figure 7 shows the morphologies of YSZ nanocrystals of varying Y_2O_3 content grown for 3 h. Regardless of composition, the nanocrystals are equiaxial in shape, and no abnormally large crystal was observed. The average nanocrystal size gradually decreased with increasing Y_2O_3 content. Although this tendency is relevant to the XRD peak broadening (Figure 4), the size is slightly larger than d_{XRD} (Figure 5a), suggesting that lattice strain remained. High-resolution TEM (HRTEM) images (Figures 8 and 9) revealed that the nanocrystals are single-crystal consisting of a well-evolved crystalline phase without an amorphous phase independent of the reaction time and Y_2O_3 content. Although lattice fringes with spacing of approximately 0.297 nm, corresponding to the (111) facet of the cubic phase or the (101) facet of the tetragonal phase, are clearly visible, the image resolution is insufficient to resolve the lattice strain.

Figure 10 shows the Raman spectra of the YSZ nanocrystals. The scattered light of shifts less than 200 cm^{-1} was removed by an optical filter. No clear Raman band except for a C_4N^+ bend

DOI: 10.1021/acs.inorgchem.5b01112
Inorg. Chem. 2015, 54, 7976−7984

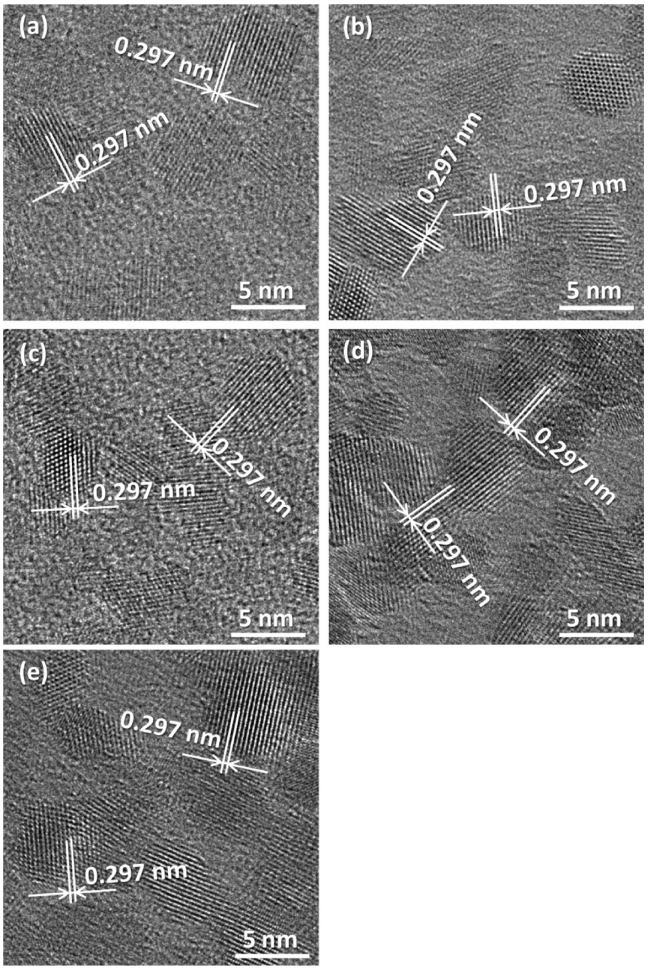

Figure 8. HRTEM images of 8YSZ nanocrystals grown at 150 °C for (a) 1 h, (b) 3 h, (c) 6 h, (d) 12 h, and (e) 24 h showing the crystalline phases with no amorphous phase and showing lattice spacing characteristics of the cubic and tetragonal phases.

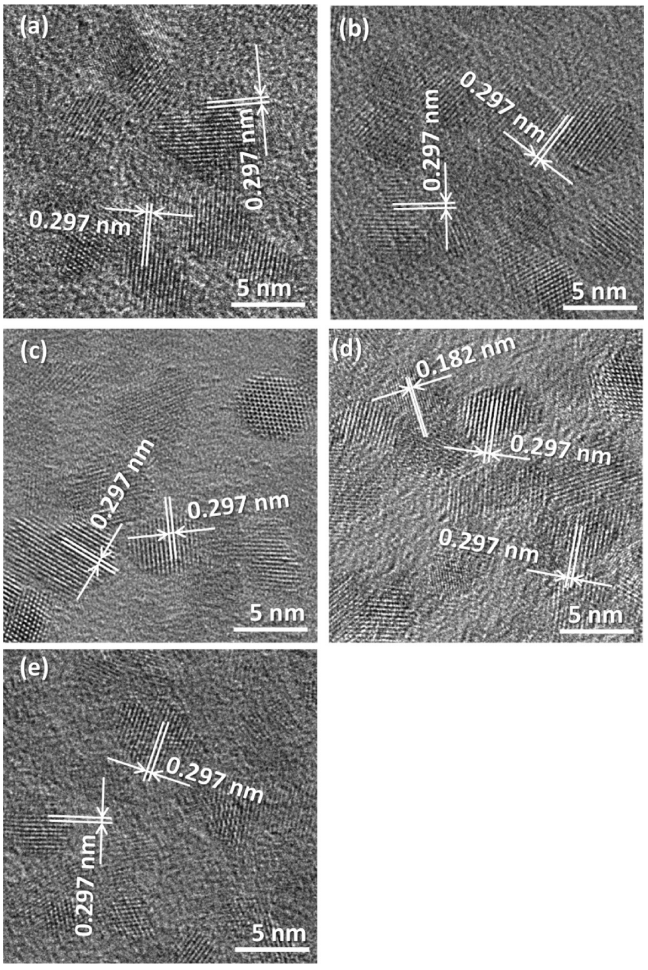

Figure 9. HRTEM images of (a) 3YSZ, (b) 6YSZ, (c) 8YSZ, (d) 10YSZ, and (d) 12 YSZ nanocrystals grown at 150 °C for 3 h showing the crystalline phases with no amorphous phase and showing lattice spacing characteristics of the cubic and tetragonal phases.

deformation (c.a. 374 cm^{-1}) and CN^+ bend deformation (c.a. 452 cm^{-1}) of $N(CH_3)_4^+$ (see Figure S-3, Supporting Information) is observed for the nanocrystals grown at 1 h independent of the composition.[25] These results strongly suggest that oxygen vacancies are randomly formed (disordered) in the lattice of YSZ nanocrystals,[26] probably due to the inhomogeneous distribution of Y^{3+} in the lattice. Inhomogeneous doping would produce the heterogeneous lattice strain, resulting in the underestimation of the particle size by XRD (d_{XRD}) (Figure 6a).[27]

The Raman bands assigned to the tetragonal phase appeared for 3YSZ after more than 3 h of reaction. The formation of a nearly pure tetragonal phase is consistent with the bulk crystal of 3YSZ, indicating that the approach employed in this study produces YSZ nanocrystals with good crystallinities. The band for the monoclinic phase appeared after 6 h of reaction, and the intensity of this band relative to those of the tetragonal phase increases with increasing reaction time. This behavior is consistent with the XRD results (Figure 4).

Only the weak bands assigned to the tetragonal phase and the broad band between 500 and 620 cm^{-1} are observed for 6YSZ after 3 h. The latter band is typically observed in bulk crystals of cubic YSZ and is attributed to the formation of disordered oxygen vacancies.[26] The band corresponding to the tetragonal phase, which is stable in the 6YSZ bulk crystal, increased with reaction time. From these results and negligible crystal growth during hydrothermal treatment (Figure 5), it is hypothesized that the nanocrystals consist of cubic phase cores and tetragonal phase shells after 3 h are formed, and then, homogenization of the Y^{3+} distribution and the resulting ordering of oxygen vacancies occurs via solid state diffusion within each nanocrystal as the reaction time is further increased.

Weak bands of the tetragonal phase and a broad band between 500 and 620 cm^{-1} appeared after 3 h and remained almost unchanged with further increases in reaction time for 8YSZ. This indicates that the cubic phase is dominant, and only a small amount of tetragonal phase is present. The phase composition agrees with the phase diagram of bulk 8YSZ crystals.[28] Only the broad band between 500 and 620 cm^{-1} is observed for 10YSZ and 12YSZ, indicating the presence of the cubic phase with a significant amount of disordered oxygen vacancies.[24]

Figure 11 shows the Y_2O_3 content of the YSZ nanocrystals determined by EDS analysis of the powdered samples. Although the Y_2O_3 content of the samples was significantly higher than the target composition when those were grown at 1 h, it steeply decreases and approaches to the target with increasing reaction time regardless of composition. This trend suggests that Y_2O_3-rich YSZ was formed at the very early stage

DOI: 10.1021/acs.inorgchem.5b01112
Inorg. Chem. 2015, 54, 7976−7984

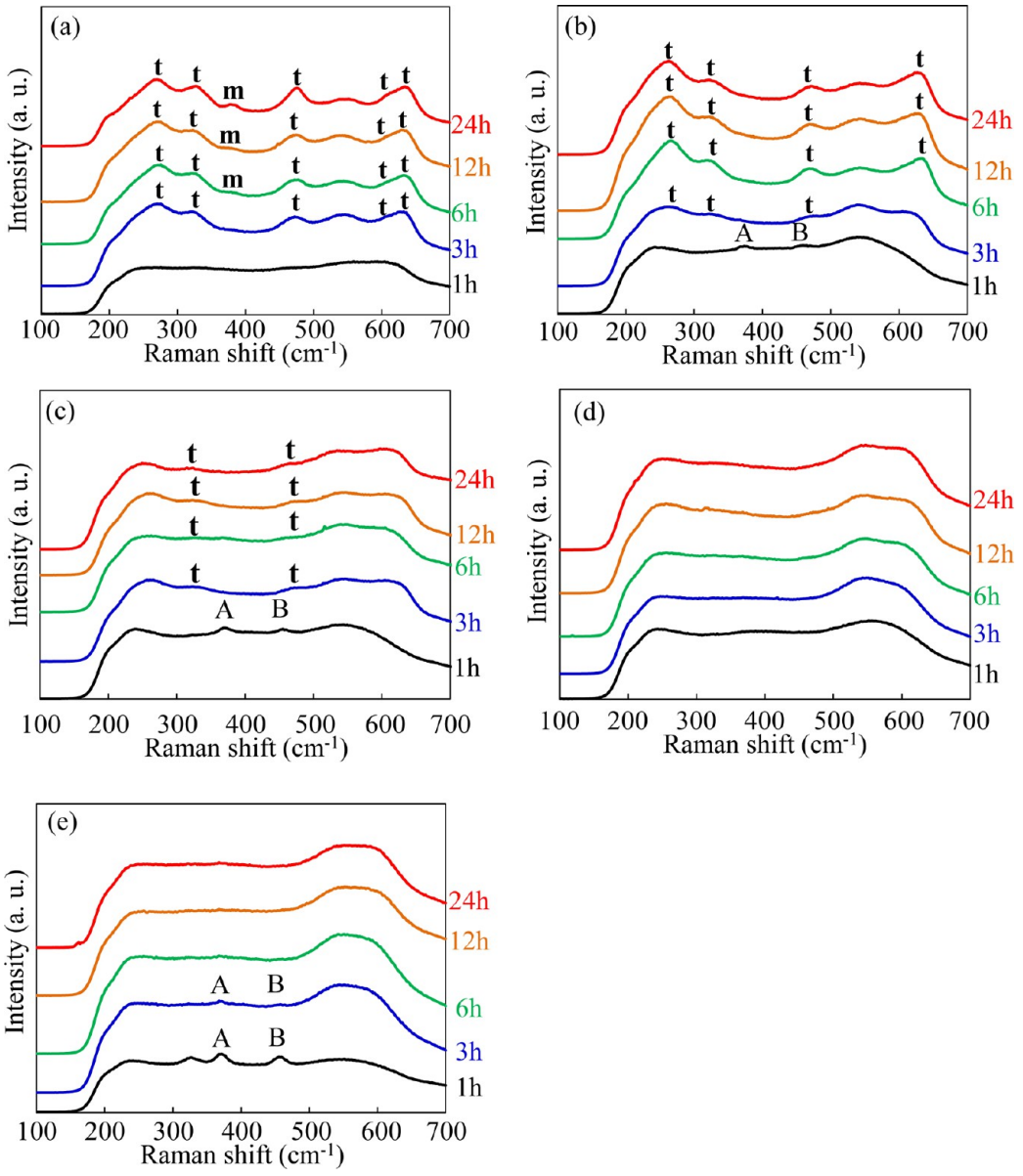

Figure 10. Raman spectra of (a) 3YSZ, (b) 6YSZ, (c) 8YSZ, (d) 10YSZ, and (e) 12 YSZ nanocrystals grown at 150 °C for 1−24 h (t: tetragonal phase; m: monoclinic phase; A: C_4N^+ deformation (bend); B: CN^+ deformation (bend)).

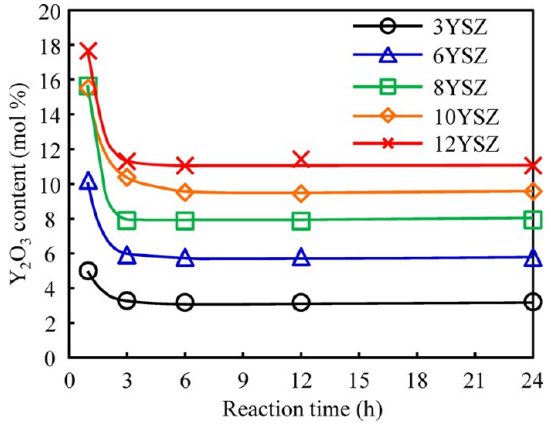

Figure 11. Effect of hydrothermal reaction time on the Y_2O_3 content of YSZ nanocrystals.

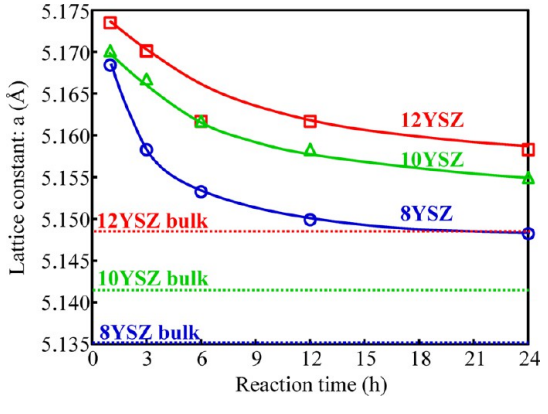

Figure 12. Effect of hydrothermal reaction time on the lattice constants determined by XRD of 8-, 10-, and 12YSZ nanocrystals.

DOI: 10.1021/acs.inorgchem.5b01112
Inorg. Chem. 2015, 54, 7976−7984

of the reaction followed by the formation of the ZrO_2-rich phase. Similar behavior was observed in the case of the growth of $Gd_{0.2}Ce_{0.8}O_{1.9}$ nanocrystals from Gd(III) and Ce(IV) carbonate complexes; the Gd_2O_3-rich phase was formed at the early stage of the reaction.[14] The smaller crystalline sizes of YSZ with higher Y_2O_3 content (see Figures 5a and 7) is probably related to the concentration of the Y(III) complex. YSZ of yttria rich phase is formed at the early stage of the reaction, suggesting the preferential conversion of soluble Y(III) complex into nuclei prior to Zr(IV) complex. On the basis of the relationship between probability of critical nuclei formation with the supersaturation (depends on the concentration),[29] the nucleation density may increase with increasing Y(III) concentration, while the amount of Zr(IV) species divided between each nuclei for growth decreases with increasing x in xYSZ. Due to the combination of higher nucleation density and lesser Zr(IV) source, the size of the nanocrystals of xYSZ with larger x may be smaller than those with smaller x.

Figure 12 shows the lattice parameter change of YSZ nanocrystals with hydrothermal reaction time. Here, 8YSZ, 10YSZ, and 12YSZ samples having cubic crystallographic symmetry (see Figure 10) were chosen, since XRD peak position can precisely be determined. While 3YSZ and 6YSZ samples were not evaluated because peak broadening in these materials masks the characteristic XRD peak splitting associated with the tetragonal phase, the XRD peak position was calibrated using silicon powder (Standard Reference Material 640e) supplied from the National Institute of Standards and Technology as the internal standard. The lattice constant monotonically decreases with increasing reaction time in all samples. The significantly larger lattice constant is the sample grown for 1 h compared with that of bulk and may be related to the formation of Y_2O_3-rich YSZ (Figure 11) since the substitution of Zr^{4+} by larger Y^{3+} causes the lattice constant to increase. However, the lattice constant continues to decrease, even after the completion of the conversion of soluble species into solids after 3 h (see Figure 3), and is almost saturated after 24 h. The continuous decrease strongly suggests that the composition is homogenized during the hydrothermal treatment. Two possible homogenization processes can be considered: dissolution/reprecipitation and solid state diffusion. Although the former should involve significant crystal growth through Ostwald ripening, no significant crystal growth was observed after 6 h (Figures 5a and 6). This strongly suggests the occurrence of a surprising phenomenon in which the solid state diffusion within each nanocrystal is the dominant homogenization process only at 150 °C. The lattice constants of the nanocrystals are slightly larger than those of the bulk crystals,[21] even after the lattice shrinkage is nearly complete after 24 h. This may be due to lattice expansion related to the unique coordination environment of the nanocrystals.[30] The lattice expansion may allow the homogenization of the composition through solid state diffusion, even under the mild conditions.

4. SUMMARY

Aqueous dispersions of YSZ nanocrystals with controlled Y_2O_3 content were successfully grown via the hydrothermal treatment of basic Zr(IV) and Y(III) carbonate complexes solutions in the presence of $N(CH_3)_4^+$. Both Y(III) and Zr(IV) complexes are converted to the solid phase with high yield regardless of the composition. Although Y^{3+} rich phase forms during the early stage of the reaction, homogenization of the composition is achieved with reaction time, apparently through solid state diffusion. Furthermore, the highly dispersed aqueous solutions of YSZ nanocrystals should be advantageous for fabricating uniform nanocomposites having advanced properties compared to the conventional composites. This approach may also be applicable to the synthesis of aqueous dispersions of trivalent lanthanide (Ln^{3+})-doped ZrO_2 nanocrystals since a variety of Ln^{3+} form similar anionic carbonate complexes.

■ ASSOCIATED CONTENT

Supporting Information

The ζ-potential of the YSZ nanocrystals of varying Y_2O_3 content grown at 150 °C for 3−24 h (Figure S-1); summary of SSA_{BET} data of YSZ nanocrystals of varying Y_2O_3 content grown at 150 °C for 3−24 h (Figure S-2); Raman spectra of (a) $N(CH_3)_4OH{\cdot}5H_2O$, (b) $N(CH_3)_4Cl$, and 12YSZ grown at 150 °C for 3 h (c) before and (d) after heat treatment at 300 °C for 6 h (Figure S-3). The Supporting Information is available free of charge on the ACS Publications website at DOI: 10.1021/acs.inorgchem.5b01112.

■ AUTHOR INFORMATION

Corresponding Author

*E-mail: kazuyoshi-sato@gunma-u.ac.jp.

Notes

The authors declare no competing financial interest.

■ ACKNOWLEDGMENTS

This work was supported by JSPS KAKENHI Grant Number 15K18210. This work was also partially supported by the Program to Disseminate the Tenure Tracking System of MEXT granted to Gunma University and by a Grant-in-Aid from the Takahashi Industrial and Economic Research Foundation. This work was performed under the Cooperative Research Program of Institute for Joining and Welding Research Institute, Osaka University.

■ REFERENCES

(1) Can, Z. Y.; Narita, H.; Mizusaki, J.; Tagawa, H. *Solid State Ionics* **1995**, *79*, 344−348.
(2) Zhao, F.; Virkar, A. V. *J. Power Sources* **2005**, *141*, 79−95.
(3) Kondoh, J.; Shiota, H.; Kawachi, K.; Nakatani, T. *J. Alloys Compd.* **2004**, *365*, 253−258.
(4) Wang, J.; Stevens, R. *J. Mater. Sci.* **1989**, *24*, 3421−3440.
(5) Jiang, S. P.; Chan, S. H. *J. Mater. Sci.* **2004**, *39*, 4405−4439.
(6) Jørgensen, M. J.; Mogensen, M. *J. Electrochem. Soc.* **2001**, *148*, A433−A442.
(7) Sato, K.; Kinoshita, T.; Abe, H. *Fuel Cells* **2010**, *10*, 320−324.
(8) Sato, K.; Kinoshita, T.; Abe, H. *J. Power Sources* **2010**, *195*, 4114−4118.
(9) Goto, Y.; Omata, T.; Otsuka-Yao-Matsuo, S. *J. Electrochem. Soc.* **2009**, *156*, K4−K9.
(10) Liu, Y.; Zhou, S.; Tu, D.; Chen, Z.; Huang, M.; Zhu, H.; Ma, E.; Chen, X. *J. Am. Chem. Soc.* **2012**, *134*, 15083−15090.
(11) Guiot, C.; Grandjean, S.; Lemonnier, S.; Jolivet, J. P.; Batail, P. *Cryst. Growth Des.* **2009**, *9*, 3548−3550.
(12) Sato, K.; Abe, H.; Ohara, S. *J. Am. Chem. Soc.* **2010**, *132*, 2538−2539.
(13) Sato, K.; Yokoyama, Y.; Valmalette, J. C.; Kuruma, K.; Abe, H.; Takarada, T. *Cryst. Growth Des.* **2013**, *13*, 1685−1693.
(14) Sato, K.; Arai, M.; Valmalette, J. C.; Abe, H. *Langmuir* **2014**, *30*, 12049−12056.

DOI: 10.1021/acs.inorgchem.5b01112
Inorg. Chem. 2015, 54, 7976−7984

(15) Takasaki, T.; Fujiwara, K.; Nakajima, Y.; Nishikawa, T.; Masu, H.; Imanari, M.; Hidaka, Y.; Ogawa, N. *Dalton Trans.* **2015**, *44*, 645−652.
(16) Janicki, R.; Starynowicz, P.; Mondry, A. *Eur. J. Inorg. Chem.* **2011**, *2011*, 3601−3616.
(17) Patterson, A. L. *Phys. Rev.* **1939**, *56*, 978−982.
(18) Brunauer, S.; Emmett, P. H.; Teller, E. *J. Am. Chem. Soc.* **1938**, *60*, 309−319.
(19) Tsai, M. C.; Tsai, T.L.; Lin, C. T.; Chung, R. J.; Sheu, H. S.; Chiu, H. T.; Lee, C. Y. *J. Phys. Chem. C* **2008**, *112*, 2697−2702.
(20) Sato, K.; Okamoto, G.; Naito, M.; Abe, H. *J. Power Sources* **2009**, *193*, 185−188.
(21) Murray, C. B.; Norris, D. J.; Bawendi, M. D. *J. Am. Chem. Soc.* **1993**, *115*, 8706−8715.
(22) Israelachivili, J. N. *Intermolecular and Surface Forces*, 2nd ed.; Academic Press: London, 1991; p 110.
(23) Guo, X. *Chem. Mater.* **2004**, *16*, 3988−3994.
(24) Ingel, R. P.; Lewis, D., III *J. Am. Ceram. Soc.* **1986**, *69*, 325−332.
(25) Michaud, P. T.; Babic, D. *J. Electrochem. Soc.* **1998**, *145*, 4040−4043.
(26) Michel, D.; Perez, M.; Jorba, Y.; Collongues, R. *J. Raman Spectrosc.* **1976**, *5*, 163−180.
(27) Zak, A. K.; Majid, W. H. A.; Abrishami, M. E.; Yosefi, R. *Solid State Sci.* **2011**, *13*, 251−256.
(28) Yashima, M.; Kakihana, M.; Yoshimura, M. *J. Am. Ceram. Soc.* **1996**, *86*−*88*, 1131−1149.
(29) De Yoreo, J. J.; Vekilov, P. G. *Rev. Mineral. Geochem.* **2003**, *54*, 57−93.
(30) Wu, L.; Wiesmann, H. J.; Moodenbaugh, A. R.; Klie, R. F.; Zhu, Y.; Welch, D. O.; Suenaga, M. *Phys. Rev. B: Condens. Matter Mater. Phys.* **2004**, *69*, 125415.

DOI: 10.1021/acs.inorgchem.5b01112
Inorg. Chem. 2015, 54, 7976−7984